Fundamental understanding of swirling flow pattern in hydrocyclones

Aurélien Davailles [a,b,*], Eric Climent [a,b], Florent Bourgeois [c]

[a] Université de Toulouse, INPT, UPS, Institut de Mécanique des Fluides de Toulouse, Allée Camille Soula, F-31400 Toulouse, France
[b] CNRS, Fédération de recherche FERMAT, Toulouse, France
[c] Université de Toulouse, INPT, UPS, Laboratoire de Génie Chimique, 4 allée Emile Monso – BP 44362, 31432 Toulouse Cedex 4, France

Keywords:
Hydrocyclone
Swirling flow
Air core
Turbulence model

A B S T R A C T

This work is concerned with establishing and validating a physics-based model that describes the swirling flow inside hydrocyclones. The physics is embedded in a Computational Fluid Dynamics (CFD) simulation model whose key features are presented and justified in the paper. Some features are selected in such a way that the model can eventually be used to simulate dense flow inside hydrocyclones. Nevertheless, its underlying physics is here within validated against dilute flow conditions. The model applies a Eulerian multi-fluid modelling approach for fluid–particle turbulent flows, and is computed using the semi-industrial code NEPTUNE_CFD. Simulation results are successfully compared to water split, velocity profiles inside the hydrocyclone and partition function measurements, either produced using our own experimental setup or from the literature. The work finds velocity profiles to be the most discriminating parameter for validation of the physics that describes the swirling flow inside the hydrocyclone. Water split on the other hand shows no relation to the choice of turbulence model and hence cannot be used to validate a mechanistic model of the hydrocyclone. The physics-based model presented here is the first building block towards describing and understanding hydrocyclone flow under dense regime.

1. Introduction

1.1. Description of particle separation

A hydrocyclone is a size classifier used to process slurries. The separation mechanism is based on enhanced gravity and takes advantage of particle size and density. Although the hydrocyclone may be used to different ends, this study is concerned with solid–liquid separation. The slurry is tangentially injected into the cylindrical zone, which provides a very high rotation rate to the slurry. Solid particles, with a higher density than the liquid, are efficiently dragged towards the outer wall by centrifugal forces induced by the curvature of streamlines (see Fig. 1).

The centrifugal acceleration can be locally several thousand times the acceleration of Earth's gravity, typically between 500 and 5000 g depending on dimensions and operating conditions of the hydrocyclone (see Section 4.5 for G-force profiles). The particulate bed that forms on the wall of the cylindrical body flows down the conical section, which ends through a narrow section tube (spigot).

The overflow (which carries fine and light particles) exits through a tube (vortex finder) that dips into the cylindrical body. The progressive downward reduction in section of the cone and the continuous increase of the solid fraction yield a significant pressure drop increase, which dictates the flow through this tube. Most hydrocyclones operate with a central air core resulting from air aspiration through the spigot; this forces the fluid and lighter particles to exit through the vortex finder.

It follows that the recovery of water to overflow or water split is generally high (around 90%). It follows that the coarser particles exit through the underflow as a dense slurry.

1.2. Computational Fluid Dynamics: a literature overview

Stepping from physical descriptions of the inner workings of the hydrocyclone, as per Bradley's 1965 classic reference work [1], Computation Fluid Dynamics (CFD) simulations of hydrocyclones did start in the 1990s. One of the early works in this field is that of Hsieh and Rajamani [2,3]. Initially, the axisymmetric assumption was imposed to reduce the simulation domain to two dimensions. The simulated water flow matched closely the fluid motion measured by Laser Doppler velocimetry inside the hydrocyclone. Qualitatively, the predictions were correct: fluid motion in rotation downward along the wall and the presence of a strong upward central vortex. Close inspection of the measurements revealed

* Corresponding author at: Université de Toulouse, INPT, UPS, Institut de Mécanique des Fluides de Toulouse, Allée Camille Soula, F-31400 Toulouse, France.
E-mail addresses: aurelien.davailles@imft.fr (A. Davailles), eric.climent@imft.fr (E. Climent), florent.bourgeois@ensiacet.fr (F. Bourgeois).

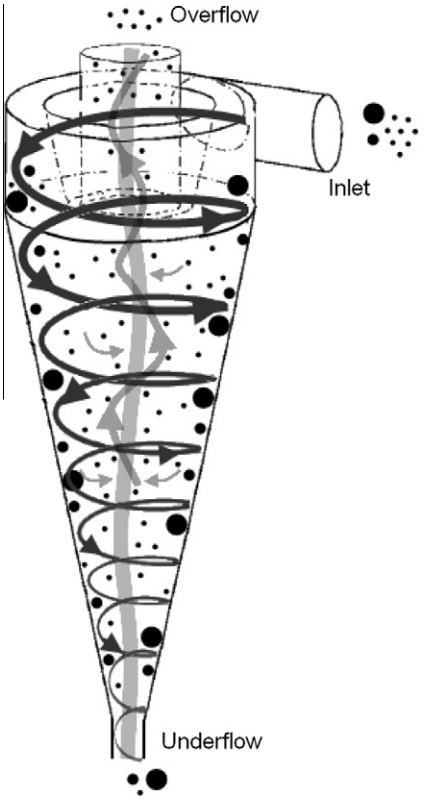

Fig. 1. Schematic of the hydrocyclone flow structure.

the presence of asymmetrical fluid flow patterns inside the device (resulting from single injection or multiple tangential injections). Consequently, the simplified symmetrical geometry was eventually surpassed by truly three-dimensional simulations. Ever since this early work, three-dimensional simulations of hydrocyclones have been improving steadily due to the continuous improvement of CFD simulation, due to improved computer technology, physical models and numerical algorithms. Nevertheless, CFD models of hydrocyclones are yet to make significant contributions in practice. There remains a great deal of scope for improving their predictive capability, which depends mostly on the quality of the physics used in the models.

All aspects of the flow cannot realistically be captured by numerical simulations due to strong turbulence, anisotropy and the three-phase nature of the flow (particles, liquid and air inside the air core). Nevertheless, the question of selecting a suitable turbulence model is an important issue. Over time, a number of significant turbulence models have been proposed: renormalization Group (RNG) [4], Reynolds Stress Model (RSM) [5] and more recently the Large Eddy Simulation (LES). Because of the strong anisotropy of the flow, the RSM model must be preferred over models that assume local isotropy of the Reynolds stress tensor. However, the precession of the air core is problematic because it contributes to the global unsteadiness of the flow. Thus, fluctuating velocity (or turbulence level) profiles are generally not accurately predicted in the central part of the flow. As shown by Slack et al. [6], LES is probably the most accurate turbulence modelling approach. It simulates the motion of high-energy vortices at large scales and applies a turbulence model at small scales.

Over the past decade, numerous publications on hydrocyclones have highlighted the importance of the presence of the air core [7–12]. A suitable method for deformable interface simulations (VOF – Volume Of Fluid) have been coupled to a RANS turbulence model or to large eddy simulation [13–16].

1.3. Objectives of the study

A number of mature empirical models have been developed over the years for assisting engineers with design or optimisation of hydrocyclones for industrial applications. It is the authors' belief that these models have evolved to a point where they can no longer be expected to help achieve significant development in hydrocyclone technology. A better understanding of the physics of flow inside hydrocyclones, which can eventually be embedded into existing empirical models is expected however to provide practitioners with new information that will help them better the performance of hydrocyclones. Enacted through CFD simulations, sound physics-based models of flow can give spatial information about hydrodynamics, like velocity profiles or solids concentration anywhere inside the hydrocyclone. Information about the inner workings of the hydrocyclone, which is difficult to obtain experimentally, will eventually help improve our understanding of hydrocyclone performance to the point where practical value can be gained from it.

The aim of our work is to propose a systematic procedure for hydrocyclones CFD simulation.

According to previous work described in Section 1.2, turbulence and air core modelling have to be taken into account through accurate models. Moreover, in order to simulate industrial cases with high feed solids content, particles should be considered.

Unfortunately, the most accurate turbulence modelling (LES) is very costly in computing time and requires algorithms with low numerical diffusion that pose numerical stability problems. Also, from a physics point of view, the validity of LES models for two-phase dense flow is still a much debated issue. The air core modelling should be done with a VOF approach, but there is no validation to date that proves the soundness of the simultaneous use of all these simulation approaches for multiphase flow. Many questions remain open regarding the reliability of coupled simulations LES-VOF with solid particles.

The work that is presented here is concerned with embedding a sound physics-based model in a CFD simulation environment that is suitable for simulation of industrial-size hydrocyclones. This implies a degree of compromise between the accuracy of the physics that is built into the model and the computational speed for solving the model; this led us to choose Eulerian multi-fluid model with RANS turbulence modelling. Simulation results have been compared to experimental data obtained on a dedicated test rig that is presented in Section 3.1. Velocity profiles published by Hsieh [3] have also been used to validate the hydrodynamics inside the hydrocyclones.

2. CFD model presentation

2.1. NEPTUNE_CFD presentation

The three dimensional numerical simulations were performed with NEPTUNE_CFD V1.07@Tlse (see [17–20]). NEPTUNE_CFD is a multiphase flow software developed in the framework of the NEPTUNE project, financially supported by CEA (Commissariat à l'Énergie Atomique), EDF (Électricité de France), IRSN (Institut de Radioprotection et de Sûreté Nucléaire) and AREVANP.

The behaviour of multiphase flows can be modelled using the general Eulerian multi-fluid balance equations. It may correspond to distinct physical materials (e.g. gas, liquid and solid particles) which can be split into different groups (e.g. water and several groups of different particles diameter); different thermodynamic phases of the same component (e.g. liquid and its vapour) or physical components, where some of which may be split into different groups. Assuming constant temperature, the following multi-fluid balance equations are obtained from the fundamental conservation laws of Physics, restricted to Newtonian mechanics:

- mass conservation
- momentum balance

These two conservation laws are written under differential form which is valid for arbitrary time and location within the continuum, except across the interfaces between two physical phases. At the interfaces, jump conditions derived from the continuous equations are written and integrated through source and sink terms in the equations.

Equations for m fluids that can be a physical phase or a model field of a physical phase, are written in a symbolic coordinate-free notation. The particular Cartesian coordinate system is used only when it makes things clearer. The algorithm, based on the elliptic fractional step method, enforces mass conservation with original pressure step actualization.

2.2. Transport equations

The multi-fluid mass balance equation for field k is written:

$$\frac{\partial}{\partial t}(\alpha_k \rho_k) + \frac{\partial}{\partial x_i}(\alpha_k \rho_k U_{k,i}) = 0 \tag{1}$$

with α_k, ρ_k, U_k, the volumetric fraction, the density and the mean velocity of phase k.

The multi-fluid momentum balance equation for phase $k$is defined as follows:

$$\frac{\partial}{\partial t}(\alpha_k \rho_k U_{k,i}) + \frac{\partial}{\partial x_j}(\alpha_k \rho_k U_{k,j} U_{k,i}) = -\alpha_k \frac{\partial P}{\partial x_i} + I_{k,i} + \alpha_k \rho_k g_i + \frac{\partial}{\partial x_j} T_{k,ij} \tag{2}$$

with P the mean pressure, $I_{k,i}$ the average interfacial momentum transfer, g_i acceleration due to gravity and $T_{k,ij}$ the effective stress tensor.

$I_{k,i}$, which accounts for momentum transfer rate from liquid to solid phase, can be modelled using an estimate of the drag force between phases (when k = l, we refer to the liquid and $k = p$ to the class p of particles).

$$I_{l,i} = -I_{p,i} = \frac{\alpha_p \rho_p}{\tau_{lp}^F} V_{r,i} \text{ with } \frac{1}{\tau_{lp}^F} = \frac{3}{4} \frac{\rho_l \langle C_D \rangle_p}{\rho_p d_p} \langle |V_r| \rangle$$

τ_{lp}^F is the viscous particle relaxation time scale and it represents the characteristic time of the interaction between fluid and particles through the drag force [21], $<>_p$ the ensemble average operator over the particulate phase. $V_{r,i}$ is the average of the local relative velocity and can be expressed in terms of the averaged velocity between phases and drift velocity (which is modelled).

The mean drag coefficient of a single particle, $\langle C_D \rangle_p$ can be written as a function of particulate Reynolds number. With several particles and in the multi-fluid approach, the particle volume fraction should be taken into account. Under these conditions, Gobin et al. [22] justifies using a combination of relations proposed by Wen and Yu [23] for dilute cases and by Ergun [24] for concentrate area regime.

$$\langle C_D \rangle_p = \begin{cases} \text{if} & \alpha_p > 0.3 \\ & Min\left[\left\langle C_D^{\text{Wen\&Yu}} \right\rangle_p ; \left\langle C_D^{\text{Ergun}} \right\rangle_p\right] \\ \text{if} & \alpha_p \leqslant 0.3 \\ & \langle C_D^{\text{Wen\&Yu}} \rangle_p \end{cases} \tag{3}$$

with

$$\left\langle C_D^{\text{Ergun}} \right\rangle_p = 200 \frac{\alpha_p}{Re_p} + \frac{7}{3}$$

$$\left\langle C_D^{\text{Wen\&Yu}} \right\rangle_p = \begin{cases} \text{if} & Re_p < 1000 \\ & \alpha_l^{-1.7} \frac{24}{Re_p}(1 + 0.15 Re_p^{0.687}) \\ \text{if} & Re_p \geqslant 1000 \\ & 0.44 \alpha_l^{-1.7} \end{cases}$$

$$Re_p = \frac{\alpha_l \rho_l d_p \langle |V_r| \rangle}{\mu_l} \tag{4}$$

2.3. Turbulence modelling

Ensemble averaging is usually applied to instantaneous Navier–Stokes equations in order to study industrial flows. It is convenient to analyse the flow into two parts: the mean (or average) flow field and fluctuations ($\tilde{u}_i = U_i + u_i$). These new equations are called Reynolds Averaged Navier–Stokes (RANS) equations. The effective stress tensor, $T_{k,ij}$, in Eq. (2) writes:

$$T_{k,ij} = \alpha_k \rho_k \langle u_{k,i} u_{k,j} \rangle + \Theta_{k,ij} \tag{5}$$

It contains two contributions: a collisional or molecular viscosity term $\Theta_{k,ij}$, respectively, for solid or liquid phases, and the turbulent kinetic stress $\langle u_{k,i} u_{k,j} \rangle$ due to turbulence or fluctuations in phase k.

2.3.1. q_k^2-ϵ_k model

The q_k^2-ϵ_k model is an extension of the classical k-ϵ model, used for single phase flow. It is a simple and widely used turbulence model that can be coupled to disperse phases (bubbles, drops or particles), but it assumes isotropy of turbulence. Using a Boussinesq hypothesis for water, the Reynolds stress tensor is expressed as follows:

$$\langle \rho_l u_{l,i} u_{l,j} \rangle_l = -\mu_l^t \left[\frac{\partial U_{l,i}}{\partial x_j} + \frac{\partial U_{l,j}}{\partial x_i}\right] + \frac{2}{3}\delta_{i,j}\left[\rho_l q_l^2 + \mu_l^t \frac{\partial U_{l,m}}{\partial x_m}\right] \tag{6}$$

introducing μ_l^t, the turbulent viscosity and the turbulent kinetic energy of the water $q_l^2 = \frac{1}{2}\langle u_{l,i} u_{l,i} \rangle_l$. As proposed by Balzer and Simonin in [25]:

$$\mu_l^t = C_\mu^* \frac{q_l^2}{\epsilon} \tag{7}$$

$$C_\mu^* = C_\mu \left[1 + C_{12} \frac{\alpha_p \rho_p}{\alpha_l \rho_l} \frac{q_l^2}{\epsilon \tau_{lp}^F}\left(1 - \frac{q_{lp}}{2q_l^2}\right)\right]^{-1}$$

with $C_\mu = 0.09$ and C_{12} = 0.34.

For the solid phase, the kinetic stress tensor, $\langle \rho_p u_{p,i} u_{pj} \rangle_p$, represents the transport of momentum by particle velocity fluctuations. The collisional stress tensor, $\Theta_{k,ij}$, accounts for transport and sink of the momentum. The constitutive relations for viscosity and diffusivity are derived in the framework of the kinetic theory of granular flows.

2.3.2. R_{ij}-ϵ_k model

The Reynold's stress model (RSM) is a second order turbulence model. With RSM, the turbulent viscosity approach has been complemented and the Reynolds stresses are computed directly. The exact Reynolds stress transport equation accounts for the directional effects of the Reynolds stress fields.

The Reynolds stress model involves calculation of the individual Reynolds stresses, $\langle \rho_k u_{k,i} u_{k,j} \rangle_k$, using differential transport equations and leads to higher computational costs. The individual Reynolds stresses are then used to obtain closure of the Reynolds-averaged momentum equation.

2.4. Computational domain

The origin of the air core comes from air being sucked through the spigot that is open to the atmosphere. The air accumulates in the area of low pressure, which forms the air core. One consequence of the presence of the air core is that it reduces the effective area available for the fluid to exit through the spigot. This reduction in section contributes to increasing the pressure drop across the hydrocyclone, which has a major effect on water split. In this work, two possible approaches have been used to model the air core. A realistic one with real gas and an economical one with a gas–liquid boundary condition replacing air in the middle of the hydrocyclone.

2.4.1. Real air-core

The first air core modelling approach we used consisted in letting the CFD model calculate the size and position of the air core inside the hydrocyclone. This was achieved by allowing air to flow upward through the spigot, as required by the Physics of the mass and momentum balance equations embedded into the CFD model. Actually, this approach mimics reality as far as the formation of the air core is concerned with a real operating hydrocyclone.

This required that the entire volume of the hydrocyclone be meshed, as shown in Fig. 2. The Simail software, which is associated with NEPTUNE_CFD V1.07@Tlse, was used to mesh the hydrocyclone. The 3D mesh was first generated by a full rotating extrusion of a vertical slice of the cyclone. Then, in order to eliminate the singularity that such a mesh generation creates in the centre of the cyclone, the central volume of the hydrocyclone was meshed as a cylinder with a concentric mesh.

2.4.2. Air-core modelling by a vertical tube

In several studies [7,11,12], the air core has been replaced by a metal rod in order to improve separation performances. This approach has been reproduced but with gas–liquid interface boundary conditions (shear free condition allowing slip). In this case, the air core is modelled by a fixed tube located at the centre of the hydrocyclone. The justification for using this air-core modelling approach is that it is clearly less computer time consuming than the first solution, which requires solving two-phase (gas–liquid) flow equations over an even greater number of cells. Mesh generation proceeded as before with Simail, meshing a vertical slice of the hydrocyclone and then a 360 degree rotation. The central hollow tube can be seen in Fig. 3.

2.5. Additional details about simulation conditions

The inlet flow assumes uniform solid concentration. In the inlet section, the Reynolds number reaches 70,000 and fully turbulent

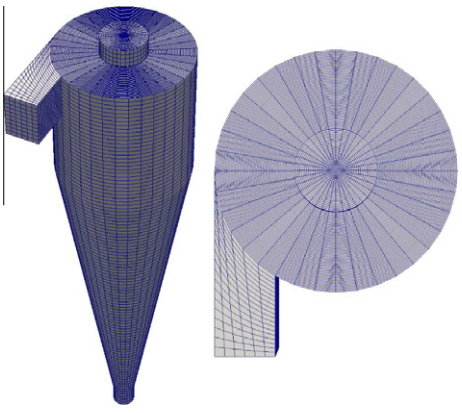

Fig. 2. Mesh with real air-core modelling.

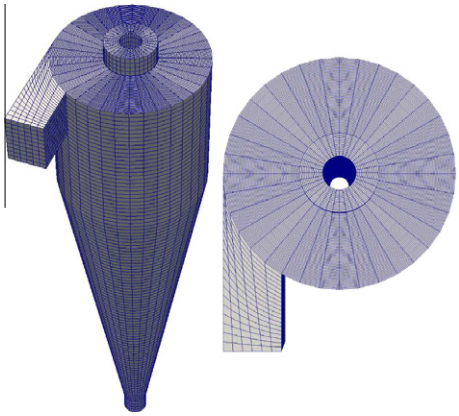

Fig. 3. Mesh with air-core modelling by a vertical tube.

conditions are used for the boundary conditions. With the tube approach for modelling the air core, shear free boundary conditions are imposed as per a gas–liquid interface (zero flux for all variables $\frac{d..}{dn} = 0$ with cancellation of the normal velocity component $U^n = 0$). Outlet boundary conditions are similar for all cases and are adapted for water and particles or for water and gas simulations. The pressure profile is imposed dynamically by copying the internal profile and resetting around a fixed pressure (atmospheric pressure) at both outlets, which allows species to enter through the underflow and overflow sections if the pressure inside the device becomes lower than atmospheric pressure. With liquid–gas simulation, only gas is allowed to enter the domain (which may occur at the spigot end of the hydrocyclone), whereas with liquid–solid simulation, the vertical tube replaces the air core and no species can flow in when the tube diameter is given its correct value.

Standard friction functions are used for the liquid phase (law of the wall) while a zero flux condition on the velocity vector is applied for particles $\left(\frac{dU_p}{dn} = 0\right)$.

The flow in the narrow section of the conical part is a critical point with meshing of the domain. Indeed, meshing the region between the air core and the spigot wall requires care. The size of the cells is almost uniform within the grid while the smallest dimension is about 2.10^{-4} m. The mesh is, respectively, composed of roughly 250,000 and 450,000 hexahedral and pentahedral structured cells for the Hsieh's hydrocyclone and for our own device. At the beginning of a simulation, the hydrocyclone is full of water. During the transient part of the simulation, water and particles are fed into the domain. Eventually, a steady-state is reached, and time averages are formed for all system variables to analyse their statistics.

3. Experimental data

Validation of the model requires access to a number of data on hydrocyclone performance. Model validation, which is covered in Section 4, relies upon measurements of water split, velocity profiles inside the hydrocyclone and partition functions. We used water split and partition functions from both our own test rig and from Hsieh [3]. Our own test rig consists of a 100 mm diameter polyurethane hydrocyclone, whereas Hsieh's used a 75 mm glass hydrocyclone. Velocity profiles used to test the physics of our CFD model are those measured by Hsieh [3].

3.1. 100 mm diameter hydrocyclone

The Neyrtec's HC100 hydrocyclone is made of interchangeable polyurethane parts, allowing various geometrical configurations to be tested (see technical specifications in Fig. 4 and in Table 1).

Table 1
General features of Neyrtec's HC100 hydrocyclone.

Model	HC 100
Diameter (mm)	100
Feed rate (m^3/h)	7–13.5
Feed pressure (bar)	0.6–2.5
Cut size (μm)	7–18
Material	Polyurethane
Overflow (mm)	33
Underflow (mm)	18

The length of the cylindrical body can be adjusted by three 100 mm extensions, and several diameter spigots (6–18 mm) are available. Only one 100 mm cylindrical extension has been installed for the data reported here, and the 18 mm diameter spigot was used. The hydrocyclone is fed using a centrifugal pump that is connected to a 1 m^3 agitated sump.

Only operating parameters and global balance (water split and partition function) are accessible with this set-up, which is not fitted with any optical means for evaluation of air core diameter.

3.2. 75 mm diameter hydrocyclone [3]

The work by Hsieh and Rajamani provides the scientific community with several sets of high quality experimental data on the flow field inside the hydrocyclone along with the first CFD model of the hydrocyclone. Not surprisingly, their experimental set-up has served as a reference configuration in many CFD studies [13,14,26–29]. The characteristics of the hydrocyclone he used are listed in Table 2.

The experimental test rig being coupled to a Laser Doppler Velocimetry measurement system, Hsieh was able to measure many velocity profiles along the height of the hydrocyclone, which we used to validate our CFD model parameter settings (pure water, 1.1 L s^{-1}). Finally, test series Nos. 7 and 8 correspond to experiments run with water and particles. Hsieh also measured and reported all the standard corresponding hydrocyclone performance data, such as water recovery to underflow or partition functions.

The hydrocyclone geometry we used in our CFD simulation work corresponded precisely to that used by Hsieh (Cf. Table 2). The cylindrical inlet tube used by Hsieh was simulated by a rectangular tube with an equivalent surface area (see [13,28,29]), which is about 8% of the cross-sectional area of the feed chamber. A sensitivity study on the inlet geometry has shown no influence of the length of the inlet pipe on hydrodynamics.

The air core diameter was estimated from the experimental velocity profiles available in Hsieh's Ph.D. paper. The air core diameter for series No. 1 (water only) is about 11 mm (88% of the spigot diameter) and 9 mm (72% of the spigot diameter) for series No. 5 (water and glycerol).

4. Model validation and analysis

The selection of both turbulence and air-core models was carried out simultaneously, as both air-core modelling techniques were tested with both k-ε and R_{ij}-ε models. The first part of our model derivation work consisted in simulating Hsieh's No. 1 series for single-phase flow, and comparing the water split and velocity profiles he measured with our CFD model predictions. Then, sensitivity tests of the numerical methodology have been realised on the two experimental geometries and the numerical and experimental separation performances have been compared with dilute slurries.

Table 2
Dimensions of Hsieh's hydrocyclone.

Cyclone diameter	75	mm
Feed diameter	25	mm
Vortex finder diameter	25	mm
Spigot diameter	12.5	mm
Length of the vortex finder	50	mm
Length of the cylindrical section	75	mm
Cone angle	20	(°)
Length of the conical section	186	mm

4.1. Water-split

For a hydrocyclone operating under continuous processing conditions with fixed inlet parameters, we first compared experimentally measured water split values with simulation results (see Table 3).

The pressure drop across the hydrocyclone is caused by the section restriction in the conical section and spigot, and by the presence of the air core. Most of the feed water flows through the vortex finder and is recovered to the overflow. For the real air-core with k-ε turbulence model, the predicted behaviour of the hydrocyclone is not relevant because there is no air sucked by the underflow. This leads to a single phase flow simulation with an equivalent CPU time (≈9 h calculation on 24 processors) to that with the tube approach.

With R_{ij}-ε turbulence model, the real air core predicted is about 10.5 mm (84% of the spigot diameter, see Fig. 5). It is very similar to air core measurements done by Hsieh and described in Section 3.2. The CPU time of this two-phase flow simulation is increased by the high gas velocity at the underflow. With the tube approach, the simulation of 2.5 physical seconds takes about 10 h on 24 processors while with the air core, the simulation of one real second takes about 17 h on the same number of processors.

Except with the combination of the real air-core model and the k-ε turbulence model, which is inaccurate, all combinations of air core and turbulence models yielded values of water split that are close to that measured by Hsieh (Table 3). These results indicate that water split carries little value for testing the validity of a CFD model

Table 3
Comparison of experimental and numerical water-split.

	Series No. 1 (water) (%)
Experimental results from [3]	95.1
Real air-core and k-ε model	73.7
Real air-core and R_{ij}-ε model	94.1
Vertical tube and k-ε model	99.0
Vertical tube and R_{ij}-ε model	92.1

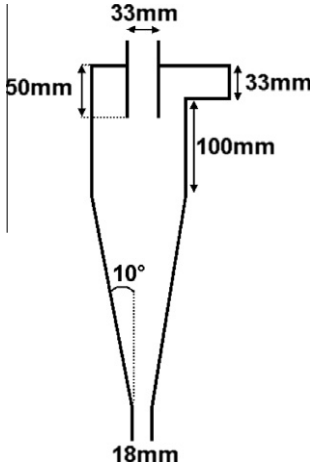

Fig. 4. Geometric features of Neyrtec's HC100 hydrocyclone.

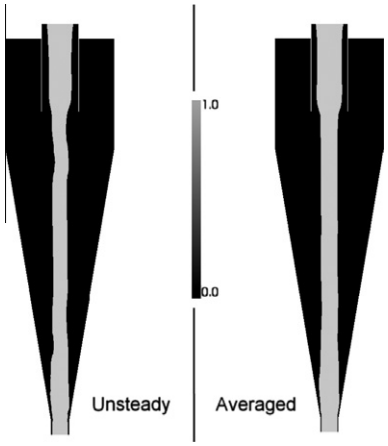

Fig. 5. Gas volume fraction with real air-core modelling and R_{ij}-ε model.

as long as the air core diameter is correctly predicted or set, as water split is a simple function of the pressure drop, which bears no relationship with the local turbulence level and mean flow structure.

4.2. Velocity profiles

Axial and tangential velocity profiles of the series No. 1 are presented in Fig. 6.

Although we saw earlier that water split predictions bore no relation to turbulence models, velocity profiles on the other hand are very much dependent on the turbulence model used in the simulations. The R_{ij}-ε model reproduces accurately axial and tangential velocity evolutions, but the k-ε model underestimates axial velocity in the centre of the cyclone and yields a poor prediction of tangential velocity resulting in a poor prediction of the pressure distribution in the central part of the device. That is the physical reason of the absence of the air core with the real air core modelling.

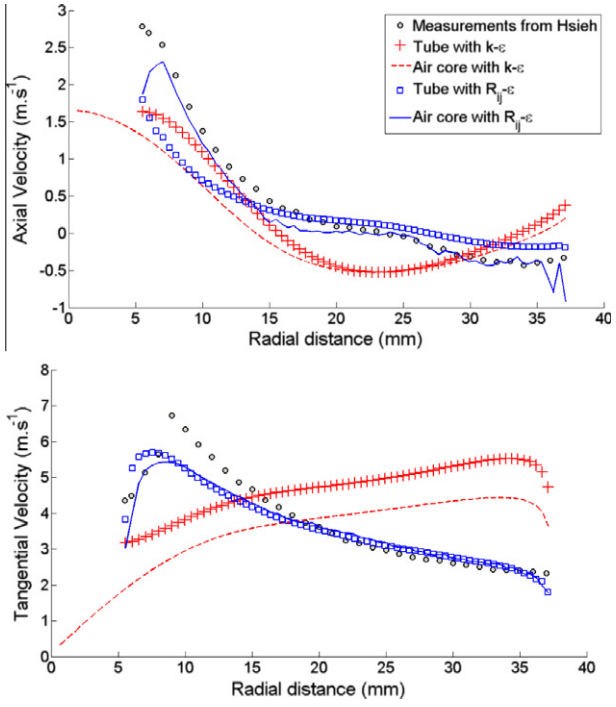

Fig. 6. Series No. 1: axial and tangential velocity profiles.

From these results, we can conclude that velocity profiles are the right parameters for selection of a suitable turbulence model, here R_{ij}-ε. In addition, since predictions with the real air-core or with the vertical tube are very close, we can also conclude that with the appropriate turbulence model modelling the air core as a constant diameter tube is suited for modelling the physics of the hydrocyclone.

4.3. Air-core: sensitivity to the tube diameter

In this section, we tested the sensitivity of the CFD model to the tube approximation of the air core for both our own hydrocyclone and that of Hsieh.

4.3.1. 75 mm diameter hydrocyclone

The question of choosing the right value of the diameter used to model the air core for any given simulation is an important issue. For the model validation above, the tube diameter was given a constant value taken from Hsieh's velocity profiles, although variations of diameter could be read along the vertical axis of the hydrocyclone (Fig. 5). The sensitivity of the separation to the value of this diameter is an important issue for the relevance of simulation results to prediction of separation performance.

The diameter of the tube was varied from 70% to 95% of the spigot diameter with the R_{ij}-ε turbulence model. The air core diameter for series No. 1, estimated through experimental profiles from Hsieh's Ph.D. thesis was about 11 mm (88% of the spigot diameter). Influence of air core diameter modelled by a rigid tube on water split can be seen in Fig. 7 under dilute conditions (1 wt% = 0.4% of silica). With too small a diameter, say less than 70% of the spigot diameter, computations lead to very low pressure at the exit (air suction). This leads to water being sucked through the spigot and reporting to the overflow, which explains the predicted increase of water recovery to overflow with small tube diameters. Increasing the diameter of the tube reduces this water suction up to a point where it becomes nil. This point, which corresponds to the right of the minimum water split value that is found in Fig. 7, is the correct tube diameter. As the diameter increases beyond this value, the surface area available for the underflow becomes too small, associated with a strong increase of the pressure drop, and the water recovery to overflow increases rapidly.

Partition curves associated with various tube diameter values within the range shown in Fig. 7 were calculated to assess the influence of the air core diameter on separation performance. We found that separation curves were only marginally sensitive to this parameter in the range 80–95%. Hence, the choice of tube diameter does not appear to be critical for prediction of hydrocyclone separation performance from CFD simulation.

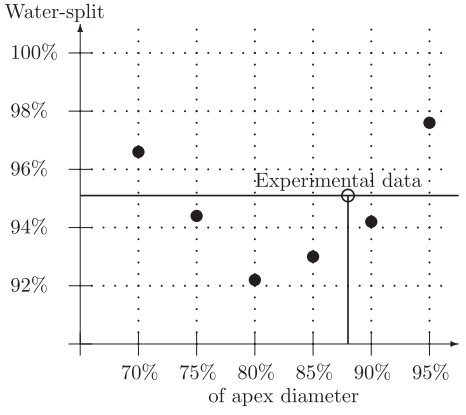

Fig. 7. Influence of tube diameter on water-split.

4.3.2. 100 mm diameter hydrocyclone

We have applied our CFD model without modifications to data of our own using a pilot test rig presented in Section 3.1.

The air core has been modelled by a vertical tube whose diameter is estimated through several simulations with different tube diameters, as explained in Section 4.3.1. It was eventually set equal to 90% of the spigot diameter (16.2 mm) (see Fig. 8).

4.4. Two-phase flow simulations

The addition of particles to our numerical simulations allowed the comparison between experimental and numerical separation performances through partition functions.

4.4.1. 75 mm diameter hydrocyclone

Two different experiments with particles are reported in [3] for dilute conditions, namely 4.88 and 10.47 wt%.

CFD simulations were performed for both cases with the R_{ij}-ε turbulence model and with a vertical tube to model the air-core. The partition functions measured by Hsieh, those predicted with our CFD model are plotted in Fig. 9. The separation curves reported here have been corrected for the water split. For instance, the total CPU time for the calculation with 4.8 wt% of silica was about 29 days. Computed on 24 processors, it represents about a calculation day.

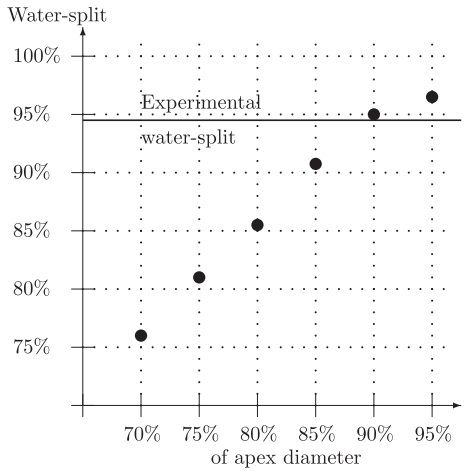

Fig. 8. Influence of tube diameter on water-split.

Overall, we find that our CFD predictions are in good agreement with the behaviour of the hydrocyclone measured by Hsieh, from the velocity profiles measured locally inside the separator to the macroscopic performance of the hydrocyclone, as seen from the water split and the partition function. These encouraging results confirm that the hypotheses and boundary conditions used for CFD simulation of the hydrocyclone capture the key features of the Physics of the separation that takes place inside a hydrocyclone under dilute conditions.

4.4.2. 100 mm diameter hydrocyclone

As our purpose is the validation of our CFD model under dilute conditions, we have restricted our presentation to the data we obtained with a 1 wt% (0.4 vol%) silica feed. Strictly identical partition curves (same cut-size and shapes) have been obtained with 5 wt% (1.9 vol%) and 10 wt% (4 vol%) feed solid content.

Measured and predicted partition functions are plotted in Fig. 10 for one particular set of operating conditions, ie for 2.25 kg s^{-1} inlet mass flow rate with 1 wt% of silica.

All things considered, the agreement between the partition functions plotted in Fig. 10 is quite remarkable. Adding to the thorough validation of the local hydrodynamics we made against Hsieh's data, this confirms that the numerical approach we have presented here for simulating hydrocyclones, which does not require any empirical parameter adjustment, yields accurate prediction of the behaviour of hydrocyclones.

4.5. Hydrodynamics of the 100 mm diameter hydrocyclone

The centrifugal force induced by the high tangential inlet velocity controls particle separation. It depends on both particle density and size (see Eq. (8)).

$$F_c = (\rho_p - \rho_l)\frac{\pi d_p^3}{6}\frac{U_{\theta p}^2}{r} \tag{8}$$

A comparison with the sedimentation force applied on particles $\left(F_g = (\rho_p - \rho_l)\frac{\pi d_p^3}{6}g\right)$ gives the G-force equals to $\frac{U_{\theta p}^2}{rg}$.

In the central part of the cyclone, where tangential velocity is highest (see tangential velocity profiles in Fig. 11 and G-force profiles at three heights for 35 μm diameter particles in Fig. 12), centrifugal force is maximum.

Velocity profiles are similar to those previously discussed in Section 4.2 and experimentally measured by Hsieh in [3]. Due to the high velocity and the low radius of curvature of the streamlines

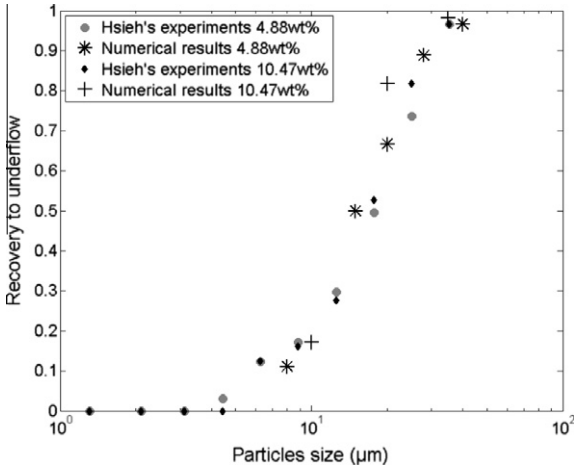

Fig. 9. Partition curve for series Nos. 7 and 8.

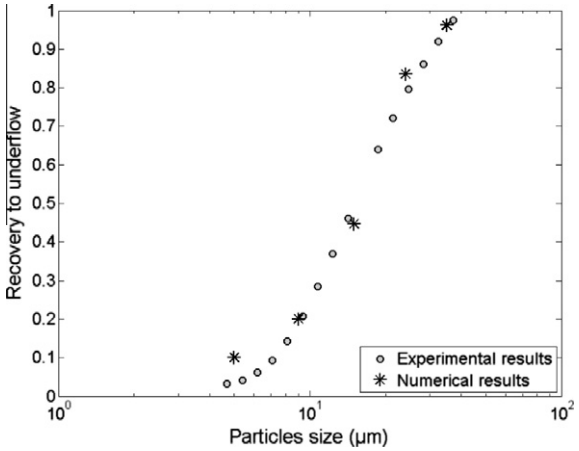

Fig. 10. Partition function for 1 wt% silica feed.

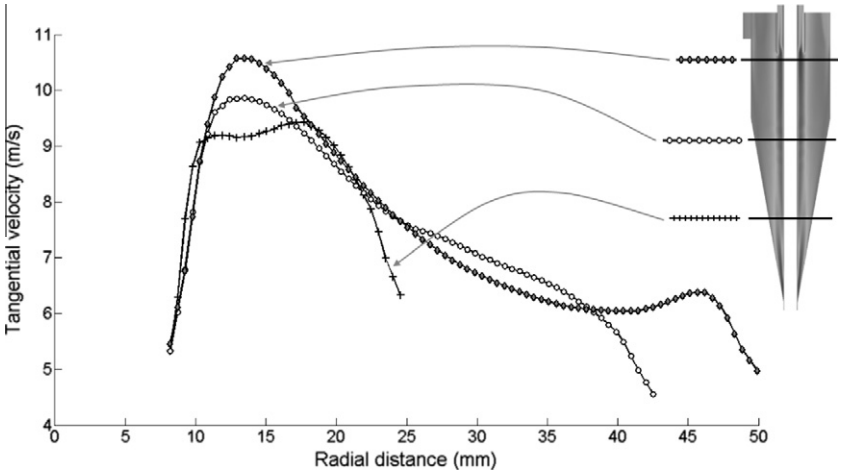

Fig. 11. Tangential velocity profiles at three hydrocyclone heights.

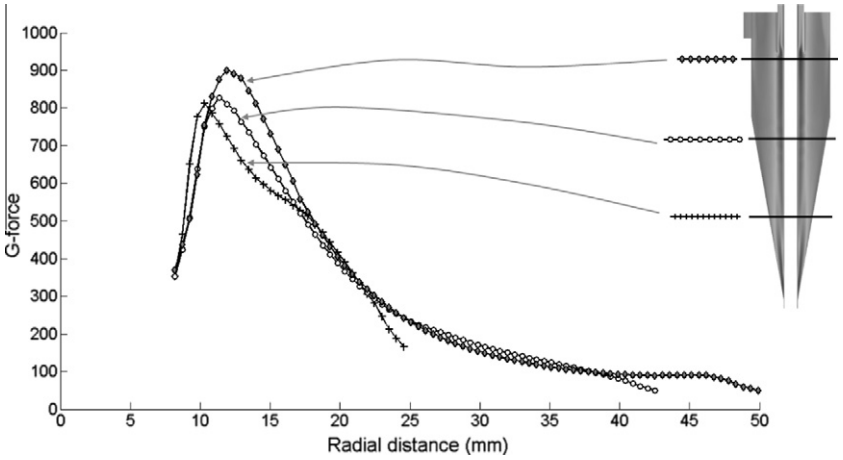

Fig. 12. G-force profiles at three hydrocyclone heights.

in the central part of the hydrocyclone, centrifugal force is very high and larger particles cannot flow towards the overflow.

Moreover, with a small amount of particles, centrifugal force is high all along the height of the device which allows radial sedimentation in the entire hydrocyclone body.

5. Conclusions and perspectives

This work aimed to derive a sound physical basis on which to build a complete CFD model of the hydrocyclone. The physics model was presented in some detail and validated against experimental data from our own pilot test rig and data from the literature. This work is the initial stepping stone towards derivation of a complete physics-based model of the hydrocyclone, and as such the proposed model is here within tested with either pure water or dilute slurries containing 1 wt% (0.4 vol%) solids. Velocity profiles inside the hydrocyclone proved to be the best criterion for testing the validity of physics assumptions. Whereas prediction of water split proved to be insensitive to the choice of turbulence model, prediction of velocity profiles on the other hand led to rejection of turbulence models which were deemed inadequate from a physics analysis of the swirling flow inside the hydrocyclone. It was found that the R_{ij}-ε model is suited for simulating the behaviour of hydrocyclones under dilute conditions. Despite the unsteady nature of the air core profile, it was found that it is possible as a first approximation to model the air core using a solid cylinder with free slip boundary condition. This clearly is computationally advantageous, and a method for choosing the correct tube diameter was proposed. It was found that the model predicted the measured partition curves, without requiring numerical fitting of the model parameters. As indicated above, this work will be followed by an upcoming publication dealing with application of the model presented here to hydrocycloning of dense slurries, whereby solids concentration has a direct influence on the performance of hydrocyclones.

Acknowledgements

The authors acknowledge TOTAL S.A. for funding this study through a Ph.D. CIFRE program and the scientific support of C. Leroi and C. Yacono. The simulations were performed at the High Performance Computing centre CALMIP (Calcul en Midi-Pyrénées) under the project P0406.

References

[1] D. Bradley, The hydrocyclone, vol. 4, Pergamon, 1965.
[2] K. Hsieh, R. Rajamani, Mathematical model of the hydrocyclone based on physics of fluid flow, AIChE Journal 37 (1991).
[3] K. Hsieh, Phenomenological model of the hydrocyclone, Ph.D. Thesis, University of Utah, Department of Metallurgy and Metallurgical Engineering, 1988.
[4] V. Yakhot, Development of turbulence models for shear flows by a double expansion technique, Technical Report, DTIC Document, 1991.

[5] B. Launder, G. Reece, W. Rodi, Progress in the development of a reynolds-stress turbulence closure, Journal of Fluid Mechanics 68 (1975) 537–566.
[6] M. Slack, R. Prasad, A. Bakker, F. Boysan, Advances in cyclone modelling using unstructured grids, Transactions of IChemE 78 (2000) 1098–1104.
[7] R. Sripriya, M. Kaulaskar, S. Chakraborty, B. Meikap, Studies on the performance of a hydrocyclone and modeling for flow characterization in presence and absence of air core, Chemical Engineering Science 62 (2007) 6391–6402.
[8] T. Neesse, J. Dueck, Air core formation in the hydrocyclone, Minerals Engineering 20 (2007) 349–354.
[9] T. Dyakowski, R. Williams, Prediction of air-core size and shape in a hydrocyclone, International Journal of Mineral Processing 43 (1995) 1–14.
[10] M. Doby, A. Nowakowski, I. Yiu, T. Dyakowski, Understanding air core formation in hydrocyclones by studying pressure distribution as a function of viscosity, International Journal of Mineral Processing 86 (2008) 18–25.
[11] R. Gupta, M. Kaulaskar, V. Kumar, R. Sripriya, B. Meikap, S. Chakraborty, Studies on the understanding mechanism of air core and vortex formation in a hydrocyclone, Chemical Engineering Journal 144 (2008) 153–166.
[12] W. Evans, A. Suksangpanomrung, A. Nowakowski, The simulation of the flow within a hydrocyclone operating with an air core and with an inserted metal rod, Chemical Engineering Journal 143 (2008) 51–61.
[13] B. Wang, A. Yu, Numerical study of particle–fluid flow in hydrocyclones with different body dimensions, Minerals Engineering 19 (2006) 1022–1033.
[14] J. Delgadillo, R. Rajamani, Exploration of hydrocyclone designs using computational fluid dynamics, International Journal of Mineral Processing 84 (2007) 252–261.
[15] K. Chu, B. Wang, A. Yu, A. Vince, CFD-DEM modelling of multiphase flow in dense medium cyclones, Powder Technology 193 (2009) 235–247.
[16] M. Brennan, CFD Simulations of hydrocyclones with an air core comparison between large Eddy simulations and a second moment closure, Chemical Engineering Research and Design 84 (2006) 495–505.
[17] A. Ozel, P. Fede, O. Simonin, 3D Numerical prediction of gas–solid flow behavior in CFB risers for Geldart A and B particles, in: Proceedings of the 20th International Conference on Fluidized Bed Combustion, 2010, PP. 805–811, doi:10.1007/978-3-642-02682-9_124.
[18] M. Galassi, P. Coste, C. Morel, F. Moretti, Two-Phase Flow Simulations for PTS Investigation by Means of Neptune CFD Code, Science and Technology of Nuclear Installations 2009 (2009) 12.
[19] J. Laviéville, O. Simonin, Equations et modèles diphasiques du code Astrid 3.4 et du code saturne polyphasique, Technical Report HE-44/99/041/A, EDF R&D, 1999.
[20] J. Laviéville, M. Boucker, M. Quemerais, S. Mimouni, N. Mechitoua, NEPTUNE_CFD V1.0 - Theory Manual, NEPTUNE Report H-I81-2006-04377-EN-Nept_2004_L1.2/3, EDF R&D, 2006.
[21] O. Simonin, Continuum modelling of dispersed two-phase flows combustion and turbulence in two-phase flows (Lecture Series 1996–02), Rhode Saint Genese, Von Karman Institute for Fluid Dynamics, 1996.
[22] A. Gobin, H. Neau, O. Simonin, J. Llinas, V. Reiling, J. Sélo, Fluid dynamic numerical simulation of a gas phase polymerization reactor, International Journal for Numerical Methods in Fluids 43 (2003) 1199–1220.
[23] C. Wen, Y. Yu, Mechanics of fluidization, in: Chemical Engineering Progress Symposium Series, vol. 62, p. 100.
[24] S. Ergun, Fluid flow through packed columns, Chemical Engineering Progress 48 (1952) 89–94.
[25] G. Balzer, O. Simonin, Three dimensional numerical prediction of two phase flow in industrial CFB boiler, in: Proceedings of the 14th International Conference on Fluidized Bed Combustion, vol. 2, pp. 1017–1022.
[26] M. Narasimha, M. Brennan, P. Holtham, Large eddy simulation of hydrocyclone – prediction of air-core diameter and shape, International Journal of Mineral Processing 80 (2006) 1–14.
[27] P. He, M. Salcudean, I. Gartshore, A numerical simulation of hydrocyclones, Chemical Engineering Research and Design 77 (1999) 429–441.
[28] B. Wang, K. Chu, A. Yu, Numerical study of particle–fluid flow in a hydrocyclone, Industrial & Engineering Chemistry Research 46 (2007) 4695–4705.
[29] B. Wang, A. Yu, Numerical study of the gas–liquid–solid flow in hydrocyclones with different configuration of vortex finder, Chemical Engineering Journal 135 (2008) 33–42.